Carbon Capture Science & Technology 2 (2022) 100027

Contents lists available at ScienceDirect

Carbon Capture Science & Technology

journal homepage: www.elsevier.com/locate/ccst

Full Length Article

Solutions of the mass continuity equation in hollow fibers for fully developed flow with some notes on the Lévêque correlation

Grigorios Pantoleontos[a,*], Ioanna Marina Anagnostara[a], Maria Syrigou[a,b], Athanasios G. Konstandopoulos[a,b,*]

[a] Aerosol & Particle Technology Laboratory, Chemical Process & Energy Resources Institute, Centre for Research & Technology Hellas (APTL/CPERI/CERTH), 6th km Charilaou-Thermi, P.O. Box 361, 57001, Thermi, Thessaloniki, Greece
[b] Department of Chemical Engineering, Aristotle University of Thessaloniki (AUTH), Thessaloniki 54124, Greece

ARTICLE INFO

KEYWORDS:
Graetz problem
separation of variables
method of lines
orthogonal collocation
SageMath

ABSTRACT

In this study a historical perspective of the mass continuity equation for fully developed laminar flow in the lumen side of a hollow-fiber membrane contactor is presented with respect to the lumen-wall boundary condition (BC). It is shown that the constant wall concentration case (Dirichlet boundary condition) imposed by the Graetz-Lévêque postulations is a sub-case of the mixed Neumann-Dirichlet linear BC largely overestimating the performance of such contactors. For the linear BC the analytical solution derived by the separation of variables method is revisited proving that it is very accurate and practical even in the region very close to the entrance of the computational domain. The analysis is extended by incorporating and solving nonlinear lumen-wall BCs with the method-of-lines approach by discretizing the radial domain using the Gauss-Jacobi orthogonal collocation and integrating the resulting initial-value differential-algebraic system. The analytical solution, the derivation of the collocation matrices and the numerical solution are presented with the aid of the open-source SageMath and the commercial package Maple.

1. Introduction

Membrane-based processes are gaining attention as an alternative to industrial well-established processes because of membrane modules' high mass transfer area (known a priori), modular design, easy scale-up [Gabelman and Hwang, 2006, Pantoleontos et al., 2010] and straightforward modelling of their flow behavior [Pantoleontos et al., 2010, Pantoleontos et al., 2017]. As shown in relevant experimental and simulation studies these membrane processes span over the whole chemical engineering curriculum, namely (membrane-based) extraction, permeation, pervaporation, reaction, perstraction, absorption, desorption and others [Qin and Cabral, 1997, Qin and Cabral, 1998]. In the following sections the model formulation of such processes is established along with the associated hypotheses taking as guide the membrane-based gas absorption process and mainly focusing on literature references on carbon capture.

This study builds upon the analytical solution of the mass continuity equation with the linear-lumen-wall BC [Pantoleontos et al., 2010] to demonstrate the implications of using reduced cases, such as the constant-concentration BC. Literature references of membrane or transport processes largely overlooked or excessively cited are incorporated and discussed throughout the text, so that analogies of the original mass transfer problem are manifested; mass transfer features and mathematical terms are underlined in association with the Graetz-Lévêque postulations, such as reaction in the lumen side, mass transfer resistances (e.g. membrane wetting), the difference between gas and liquid flow in the lumen side with respect to the Graetz dimensionless number, entrance-region versus separation-of-variables analytical solutions and others.

Apart from the linear-BC case numerical analysis is extended to nonlinear BCs, for which the method of lines is applied by discretizing the radial domain using the Gauss-Jacobi-Lobatto orthogonal collocation method and integrating the resulting initial-value differential-algebraic system. All cases demonstrations are provided in a step-by-step hands-on approach with the aid of current computational tools, such as the open-source [SageMath, 2021] and the commercial software [Maple, 2021], so that the reader may directly validate the code and compare with other available approximations.

* Corresponding author.
E-mail addresses: pantole@certh.gr (G. Pantoleontos), anagnostara@certh.gr (I.M. Anagnostara), msyrigou@certh.gr (M. Syrigou), agk@certh.gr (A.G. Konstandopoulos).

https://doi.org/10.1016/j.ccst.2021.100027
Received 15 November 2021; Received in revised form 27 December 2021; Accepted 29 December 2021

Nomenclature

$A_{i,j}$, $B_{i,j}$	collocation matrices
a_k	parameters for the nonlinear BCs, k=1..4
C	concentration of the diffusing component in the lumen (mol/m^3)
C_0	lumen initial concentration of the diffusing component (mol/m^3)
c_n	Fourier coefficients of the analytical solution
C_s^*	shell-side concentration at the module end where the lumen fluid enters
$C_{s,z}$	concentration of the diffusing component in the solvent of the shell side (mol/m^3)
$\hat{C}$	lumen dimensionless concentration
C_{mc}	lumen mixed-cup concentration (mol/m^3)
C_{mc}^*	dimensionless lumen mixed-cup concentration
D	diffusion coefficient of the diffusing component in the lumen (m^2/s)
G_z, G_z'	Graetz numbers
$H_{A,solv}$	Henry's constant of the dissolved gas (Pa·m^3/mol)
$J_N^{\alpha,\beta}$	Jacobi polynomials of N-th degree with a, β, coefficients
K_{ext}	combined (shell and membrane) mass transfer coefficient (m/s)
m	equilibrium coefficient
n	number of eigenvalues of the analytical solution
N	interior collocation points
N_f	number of fibers
Nu	Nusselt number
Pe	Péclet number
$p_{N+2}(\hat{r})$	N+2 degree (node) polynomial
Q_g	volumetric flowrate at the lumen's inlet (m^3/s)
r	radial distance (m)
$\hat{r}$	dimensionless radial distance
R	gas constant (Pa·m^3/mol/K)
R_f	fiber radius (m)
R_m	membrane mass transfer resistance (s/m)
R_s	shell-side mass transfer resistance (s/m)
$Sh_{avg,z,o}$	logarithmic averaged overall Sherwood number
$Sh_{avg,z}$	logarithmic averaged lumen Sherwood number
Sh_w	Sherwood number at the fiber wall
Sh_z	local lumen Sherwood number
T	temperature (K)
u	lumen average velocity (m/s)
u_z	lumen axial velocity (m/s)
w_i	Lobatto weights of the orthogonal collocation method
z	axial distance (m)
$\hat{z}$	dimensionless axial distance, inverse Gz number
$\Gamma(x)$	gamma function
Λ_n	eigenvalues of the analytical solution
$M(a,b,x)$	Kummer's function

2. Theory

2.1. Model formulation

Guided by the membrane-based gas absorption process, the flowing behavior is depicted in Figure 1, where the gas mixture flows in the fiber (lumen) side and the absorbing medium outside of the fibers, in the shell side, in counter-current mode of operation. For this type of process the membrane does not introduce any selectivity to one gas species over the other: the extent of the separation of the mixture depends on the solubility difference of the species into the selected shell-side liquid solvent [Rongwong et al., 2012], and especially on whether gas-liquid reactions take place. The following assumptions are made to describe the fluid flow within the fiber and the transport of the diffusing component through the membrane pores: (a) isothermal operation; (b) Newtonian fluids physical properties; (c) fully developed, laminar flow in the lumen (fiber); (d) applicability of Henry's law; (e) since the velocity profile is fully developed, the velocity term in radial direction is zero [Skelland, 1974]; (f) the axial molecular diffusion is neglected once the Peclet number is greater than 100 [Kim and Stroeve, 1988].

Considering the assumptions above, the continuity equation in a fiber (lumen side) for a single component becomes:

$$2 \cdot u \left[1 - \left(\frac{r}{R_f}\right)^2\right] \frac{\partial C}{\partial z} = D\left[\frac{1}{r}\frac{\partial}{\partial r}\left(r\frac{\partial C}{\partial r}\right)\right] \quad (1)$$

with the associated boundary conditions (see also Figure 1): C(z, r) =C_0

$$\left.\frac{\partial C}{\partial r}\right|_{z,r=0} = 0 \quad (2)$$

(symmetry boundary condition at the fiber center) (3)

$$-D\left.\frac{\partial C}{\partial r}\right|_{z,r=R_f} = K_{ext}\left[C\left(z, r = R_f\right) - mC_{s,z}\right] \quad (4)$$

where u is the average velocity in the lumen, C is the concentration of the diffusing component, C_0 is the initial concentration, D is the diffusion coefficient of the diffusing component and $C_{s,z}$ is the concentration of the diffusing component in the solvent of the shell side.

Figure 1 also shows where each boundary condition is located. The BC at r=R_f (inner radius of a fiber) of Equation (4) is a mixed Neumann-Dirichlet (or frivolously, Robin [Gustafson and Abe, 1998]) BC: it is linear if the mass transfer and the diffusion coefficients do not depend on the lumen concentration, or the shell-side concentration, $C_{s,z}$, does not vary with z-direction. For nonlinear or integro-differential lumen-wall BCs the reader is referenced to Qin and Cabral [1998] and Pantoleontos et al. [2010, 2017] (and references mentioned therein), while a set of nonlinear BCs is discussed and solved in subsequent sections of this work. Furthermore, the linear BC (4) is further analyzed in the following section with the aid of the Graetz-Lévêque postulations in order to enunciate the arguments and the motivation of the current study.

The term m is the partition coefficient of the diffusing component corresponding to equilibrium conditions between the lumen and shell fluids depending on the physical properties of the fluids – cf. membrane-based extraction [Pantoleontos et al., 2010, Mavroudi et al., 2003]. The relationship between gas-solvent dimensionless partition coefficient, m, and Henry's constant, $H_{A,solv}$, for a solute is given by the following expressions [Vallero, 2014]:

$$m = \frac{C}{C_{s,z}} = \frac{H_{A,solv}}{RT} \quad (5)$$

where $H_{A,solv}$ is the Henry's constant of the dissolved gas (indicative units: Pa·m^3/mol), R is the gas constant (Pa·m^3/mol/K), and T is temperature (K).

So far, by solving the continuity equation (1) with the associated BCs (2)-(4) the lumen concentration variation in two dimensions is fairly defined. For the original case depicted in Figure 1, the external mass transfer coefficient, K_{ext}, includes all relevant mass transfer resistances and regions of transport between the membrane and the shell-side boundary layer, *from where the lumen (gas) mass transport resistances end*, i.e. the membrane itself, including any partial wetting imposed by the penetrating liquid into the membrane pores [Cao et al., 2021], and the shell-side concentration boundary layer including any enhancement factor in the case of a reactive mixture:

$$\frac{1}{K_{ext}} = R_m + R_s \quad (6)$$

where R_m and R_s are the membrane and the shell-side mass transfer resistances, respectively. An additional mass transfer resistance in such

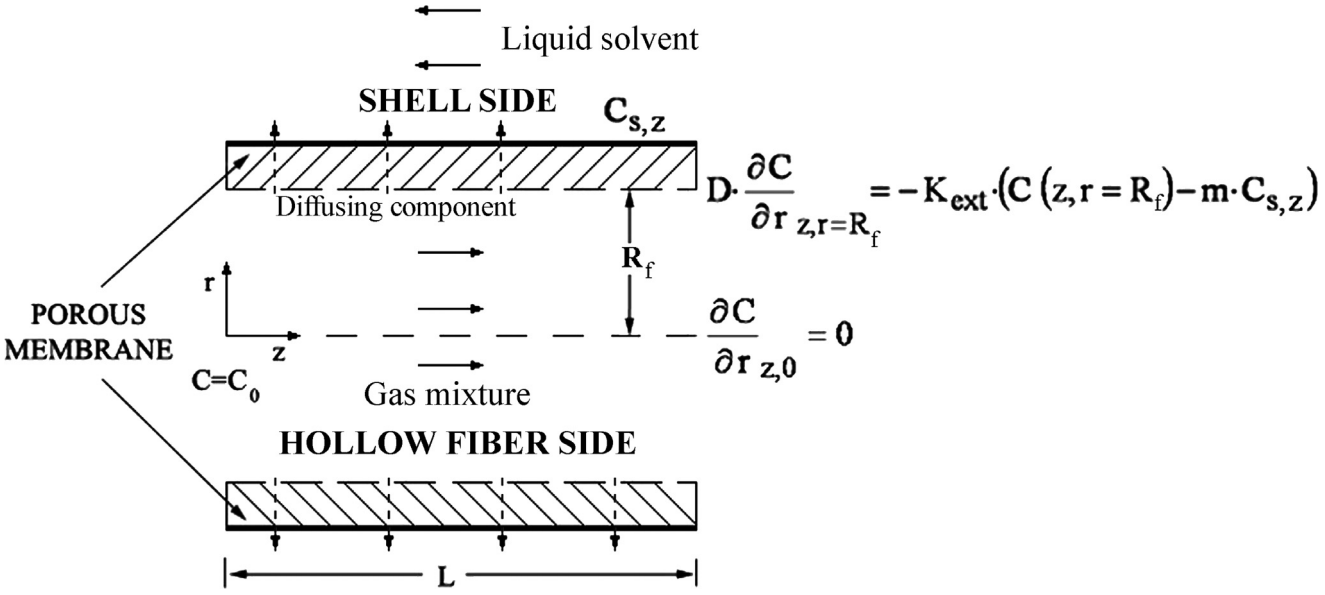

Figure 1. A single hollow fiber flow pattern with gaseous mixture flowing in the lumen-side and counter-current mode of operation depicting the corresponding boundary conditions (adapted from [Pantoleontos et al., 2017]).

processes is imposed by liquid penetration into the membrane pores, so that the membrane resistance needs to be further resolved into its constituent parts accounting for the extent of wetting, the gas-filled portion and the liquid-filled part of the pores resistance [Pantoleontos et al., 2017] and references mentioned therein. It has to be noted that the same mathematical formulation holds (with exactly the same sign in the lumen-wall BC) if the gas flows in the shell side and the liquid flows in the lumen side provided that no reaction takes place in the lumen side.

The lumen-side gas mixture average velocity for a cylindrical fiber is found by

$$u = \frac{Q_g}{N_f \pi R_f^2} \tag{7}$$

where Q_g is the volumetric flowrate at the lumen's inlet and N_f is the number of fibers.

In the preceding analysis, the shell-side concentration of the diffusing component from the lumen through the membrane pores is supposed to be constant, a major assumption in the postulated model: for the general case of shell-side non-constant concentration one has to solve the mass balance in the shell side, which in principle derives an integro-differential lumen-wall BC [Qin and Cabral, 1997].

The shell-side mass transfer coefficient from which the shell-side resistance, R_s, is calculated can be found from relevant correlations taking into account the configuration of the module (e.g. either parallel or cross-flow modules). Analytical solutions for the shell side for parallel flow modules using Happel's free surface model and Dirichlet BCs at the fiber's outer diameter can be found in [Zheng et al., 2003]. For cross-flow modules the determination of the hydraulic diameter must take into account the void area of the mixing flow space, while the mean shell-side velocity is calculated by a much more complicated expression taking also into account the porosity, ε, of the bed, i.e. the interstitial velocity (see e.g. [Schöner et al., 1998, Mahmud et al., 2000]).

Following Qin and Cabral [1997] and Cooney et al. [1974] the dimensionless variables $\hat{r} = r/R_f$, $\hat{C} = (C - mC_s^*)/(C_0 - mC_s^*)$, $\hat{z} = zD/(4uR_f^2) = {}^1/_{Gz}$, $Sh_W = 2K_{ext}R_f/D$ are introduced, so that the preceding system of partial differential equations (1)-(4) is rendered dimensionless:

$$(1 - \hat{r}^2)\frac{\partial \hat{C}}{\partial \hat{z}} = \frac{2}{\hat{r}}\frac{\partial \hat{C}}{\partial \hat{r}} + 2\frac{\partial^2 \hat{C}}{\partial \hat{r}^2} \tag{8}$$

$$\hat{C}(0,\hat{r}) = 1 \tag{9}$$

$$\frac{\partial \hat{C}}{\partial \hat{r}}_{\hat{z},0} = 0 \tag{10}$$

$$\frac{\partial \hat{C}}{\partial \hat{r}}_{\hat{z},1} = -\frac{Sh_W}{2}\hat{C}(\hat{z},1) \tag{11}$$

Membrane processes subject to assumptions (a)-(f) that can be described by Eqs. (8)-(11) are categorized by Qin and Cabral [1997]. It is worth mentioning that for these processes the same mathematical methodology and solutions are applied. The dimensionless lumen mixed-cup concentration, C_{mc}^*, depends only on $\hat{z}$ and is defined as Qin et al. [1996]:

$$C_{mc}^*(\hat{z}) = \frac{C_{mc}(z) - mC_s^*}{C_0 - mC_s^*} = 4\int_0^1 (1 - \hat{r}^2)\hat{r}\hat{C}(\hat{z},\hat{r})\partial\hat{r} \tag{12}$$

since [Koutsonikolas et al., 2021]

$$C_{mc}(z) = \frac{\int_0^{R_f} 2\pi r u_z \cdot C(z,r)\partial r}{\int_0^{R_f} 2\pi r u_z \partial r} = \frac{4}{R_f^2}\int_0^{R_f} r\left(1 - \left(\frac{r}{R_f}\right)^2\right)\cdot C(z,r)\partial r \tag{13}$$

The logarithmic averaged overall and lumen Sherwood numbers, $Sh_{avg,z,o}$ and $Sh_{avg,z}$, respectively, and the local lumen Sherwood number, Sh_z, are given by Qin and Cabral [1997]:

$$Sh_{avg,z,o}(\hat{z}) = -\frac{ln\left(C_{mc}^*(\hat{z})\right)}{4\hat{z}} \tag{14}$$

$$\frac{1}{Sh_{avg,z}(\hat{z})} = \frac{1}{Sh_{avg,z,o}(\hat{z})} - \frac{1}{Sh_W} \tag{15}$$

$$Sh_z(\hat{z}) = \frac{-2\frac{\partial \hat{C}}{\partial \hat{r}}_{\hat{z},1}}{C_{mc}^*(\hat{z}) - \hat{C}(\hat{z},1)} \tag{16}$$

From the above analysis it is evident that membrane processes (as every chemical engineering process) are affected by transport resistances which are present within the different phases and across the interacting interfaces: the magnitude of these resistances determines the mathematical model and its BCs. In the following section a historical review of the Graetz problem is presented and the inner-wall BC is scrutinized; it

Table 1
Application of the "Lévêque correlation" Eq. (17) in the gas-liquid contact membrane literature with emphasis on CO_2 capture.

Reference	Notes
Kumar et al. [2003]	The authors confirm that there are no mass transfer resistances and the Gz number is adequately high, so that the Lévêque correlation used is valid. CO_2 capture with water, NaOH. Polypropylene (PP) membranes. Liquid through the lumen side.
Dindore et al. [2004]	The authors find that the Lévêque solution describes very well the experimental behavior of CO_2 capture with water and propylene carbonate, but not with n-formyl morpholine. The discrepancy is attributed to wetting. The authors acknowledge the relation of the correlation application with the absence of external mass transfer resistance. Polytetrafluoroethylene (PTFE) and PP membranes. Liquid through the lumen.
Dindore et al. [2004]	Pressure conditions up to 20 bar. The authors find that the Lévêque solution describes very well the experimental behavior for propylene carbonate at elevated pressures, but not at atmospheric conditions. The discrepancy is attributed to wetting. The authors confirm that Gz number is small for their experimental conditions and they acknowledge the relation of the correlation application with the absence of external mass transfer resistance. PP membranes. Liquid through the lumen.
Dindore and Versteeg [2005]; Dindore et al. [2005]	CO_2 capture with water. PP membranes. Liquid through the lumen.
Atchariyawut et al. [2007]	Possibility of membrane wetting. Biogas upgrading using water, NaOH, monoethanolamine (MEA), and NaCl as an additive in the NaOH aqueous solution. Polyvinylidene difluoride (PVDF) membranes. Liquid through the lumen.
Lu et al. [2008]	Membrane wetting (resistance-in-series model). CO_2 capture with methyl-diethanolamine (MDEA). Polymeric membranes. Liquid through the lumen.
Lin et al. [2009]	Membrane wetting (resistance-in-series model). CO_2 capture with piperazine (PZ), MDEA, and aminomethyl-propanol (AMP). PP or PVDF membranes. Gas mixture through the lumen.
Mansourizadeh and Ismail [2009]	Review of acid gas capture. Generalized by Kreulen et al. [1993] Graetz-Lévêque correlation.
Portugal et al. [2009]	Generalized by Kreulen et al. [1993] Graetz-Lévêque correlation. CO_2 capture with potassium glycinate. PDMS (polydimethylsiloxane) membranes. Liquid through the lumen.
Rongwong et al. [2012]; Rongwong et al. [2009]; Rongwong et al. [2013]; Rongwong et al. [2015]	Membrane wetting. CO_2 capture with water, MEA, diethanolamine (DEA), AMP, sodium glycinate (SG), NaCl. PTFE or PVDF membranes. Liquid through the lumen.
Scholes et al. [2012]	Membrane wetting (resistance-in-series model). CO_2 capture with MEA, K_2CO_3. PP and PTFE membranes. Either gas or liquid mixture through the lumen.
Cui et al. [2015]	Membrane wetting (resistance-in-series model). CO_2 capture with DEA. PVDF membranes. Liquid through the lumen.
Boributh et al. [2011]] Boributh et al. [2013]	Membrane wetting. CO_2 capture with water or MEA. PP or PVDF membranes. Gas or liquid through the lumen.
Rahbari-Sisakht et al. [2012]	Membrane wetting. CO_2 capture with water, NaOH. Porous asymmetric polyetherimide (PEI) membranes. Liquid through the lumen ($400<Gz<1500$).
Wang et al. [2013]	Membrane wetting. Generalized by Kreulen et al. [1993] Graetz-Lévêque correlation. CO_2 capture with MEA, DEA, MDEA. PP hollow fibers. Liquid through the lumen.
Bougie et al. [2014]; Iliuta et al. [Iliuta et al., 2015]	CO_2 capture with either 2-amino-2-hydroxymethyl-1,3-propanediol (AHPD)+ PZ, or MEA, MDEA, AMP. PTFE membranes. Liquid through the lumen.
Jin et al. [2017]	Biogas upgrading by removing CO_2 and H_2S using water, potassium sarcosine (PS), MEA, KOH and K_2CO_3. PVDF membranes. Gas mixture through the lumen.
Li et al. [2017]	Elevated pressures. CO_2 capture with polyethylene glycol dimethyl ether (Selexol). PTFE membranes. Liquid through the lumen.
Ghobadi et al. [2018]	CO_2 capture with MEA and DEA. PTFE membranes. Gas mixture through the lumen.
Nakhjiri et al. [2018]	Lévêque correlation in the shell side. Biogas upgrading using MEA and triethanolamine (TEA). PP membranes.
Xu et al. [2019]	The Lévêque correlation is suggested to be used in the shell side. The cited references [Yang and Cussler, 1986, Gabelman and Hwang, 1999] do not indicate that this correlation is used in the shell, but in the fiber.
Lee et al. [2020]	The pre-exponential parameter in Eq. (17) is substituted for 1.615 [see Eq. (18)]; also, a typographical error in the exponent (1/2 instead of 1/3). Stripping of CO_2 from MEA solution. Ceramic hollow fiber membranes. Liquid with dissolved CO_2 either through the shell or the lumen.
Nakhjiri and Heydarinasab [2020]	Lévêque correlation in the shell side. CO_2 capture with potassium lysinate (PL) amino acid solution.
Cao et al. [2020]	Membrane wetting. CO_2 capture with 4-diethylamino-2-butanol (DEAB). PTFE membranes. Liquid through the lumen.
Houlker et al. [2021]	Extended discussion of the application of the Lévêque correlation including mass transfer correlations in the shell side. CO_2 capture with water. PP membranes. Liquid through the lumen.

is shown that the problem can be reduced to a constant wall concentration BC under certain and fundamental requisites. Afterwards, the dimensionless problem with the linear BC is analytically solved, while extensions into nonlinear BCs are also presented.

2.2. The cult of the Lévêque correlation

Membrane contactors' literature features stock models for the description of the flow behavior within the fibers, which are summarized as the Graetz-Lévêque (or merely Lévêque) correlation(s) by a vast number of researchers [Rongwong et al., 2012, Kumar et al., 2003, Dindore et al., 2004, Dindore et al., 2004, Dindore and Versteeg, 2005, Dindore et al., 2005, Atchariyawut et al., 2007, Lu et al., 2008, Lin et al., 2009, Mansourizadeh and Ismail, 2009, Portugal et al., 2009, Rongwong et al., 2009, Rongwong et al., 2013, Rongwong et al., 2015, Scholes et al., 2012, Cui et al., 2015, Boributh et al., 2011, Boributh et al., 2013, Rahbari-Sisakht et al., 2012, Wang et al., 2013, Bougie et al., 2014, Iliuta et al., 2015, Jin et al., 2017, Li et al., 2017, Ghobadi et al., 2018, Nakhjiri et al., 2018, Xu et al., 2019, Lee et al., 2020, Nakhjiri and Heydarinasab, 2020, Cao et al., 2020, Houlker et al., 2021] as Table 1 demonstrates (limited to gas-liquid contact membrane literature with emphasis on CO_2 capture):

$$Sh = 1.62 \cdot Gz^{1/3} \tag{17}$$

Apart from the historical interest, as the "Lévêque correlation" becomes ubiquitous in the membrane modelling canon – see also a review by Wang et al. [2017] – it is the underlying assumptions leading to the analytical expressions that are binding when applying them to a specific problem. As the main uncertainty lies on the BC at the inner wall which describes the flux through the (membrane) wall and implicitly determines the flow along the fibers, it needs to be carefully assigned: for the following discussion the mixed Neumann-Dirichlet BCs Eqs. (4) and – equivalently in dimensionless form – (11) will be the reference case, from which the Dirichlet BC may be derived.

Consider the case when the dimensionless number $K_{ext}R_f/D$ (Sherwood number) has a very large – infinite – value at the boundary, that is, zero transport resistance. Intuitively, if the fluid in motion has no resistance to overcome, it gets the same concentration value at both sides of the non-resistant wall, accounting for the equilibrium

coefficient, $C(z, r = R_f) = mC_{s,z}$: a Dirichlet BC (see also discussion in [Kooijman, 1973, Shah and London, 1978]).

The equivalent heat transfer problem with the corresponding Dirichlet BC (along with the assumptions (a)-(f) still holding) has been studied in principle and solved by Graetz in 1883, who derived an infinite series solution. Since the calculation of the required eigenvalues was very tedious back then, Graetz was able to derive the first three eigenvalues [Knudsen and Katz, 1958], while Brown later on presented eleven eigenvalues [Brown, 1960]. Interestingly and most revealingly, the analytical solution presented by Pantoleontos et al. for Eqs. (8)-(11) (mixed Neumann-Dirichlet BC) with Sh_W equal to 10^{14} (practically infinity) derives exactly the same eigenvalues with those presented by Brown [Pantoleontos et al., 2010, Brown, 1960] (see also relevant discussion regarding Brown's solution and values in [Kooijman, 1973, Kays and Crawford, 1993, Glasgow, 2010, Ghiaasiaan, 2011]): thus, it is also numerically confirmed that the mixed Neumann-Dirichlet BC case when the wall resistance is zero is reduced to the Graetz problem imposing the Dirichlet BC (see also discussion in Qin et al. [1996]). Eloquently, if assumptions (a)-(f) can adequately postulate the flow model, one should use the "general-case" BC (4), calculate the physical properties of the fluids, determine the membrane and shell-side transfer coefficients etc., so that the value of the combined mass transfer coefficient, K_{ext} and the associated dimensionless Sh_W are established: if they are calculated to be very large, then the Dirichlet BC – Graetz problem – naturally emerges.

The tricky part of the separation-of-variables method which yields the analytical solution in terms of the infinite-series expansion (including the analytical solution derived by Pantoleontos et al. for the "general-case" BC (4) [Pantoleontos et al., 2010]) is that for small $\hat{z}$-values ($\hat{z} < 0.01$, that is, high Gz numbers), quite a lot of eigenvalues need to be determined for the accurate calculation of the logarithmic averaged overall and local lumen Sherwood numbers [Pantoleontos et al., 2010] – in the remaining length six eigenvalues are enough. (In the subsequent sections it is shown that this analytical solution on which the current study is based is still very accurate and practical for $\hat{z} \geq 0.000025$, and apparently it should be used with certainty in all practical situations for this kind of processes).

Lévêque alleviated this shortcoming by presenting an analytical solution using the similarity transformation [Salazar et al., 1988], which is valid only in the entrance region – still using the Dirichlet BC at $r=R_f$ [Churchill, 2013], while BC (3) is no longer needed [Shih and Tsou, 1978]. (The ingenuity of Lévêque to apply this particular transformation is vividly described by Churchill, [2000]). Newman extended Lévêque solution (adding two more terms) for mass transfer in fully developed laminar flow in cylindrical coordinates – still with constant wall concentration as a BC and valid only for the beginning of the mass transfer region [Newman, June 1967], that is, for small $\hat{z}$ values:

$$Nu = 1.6151 \cdot \left(\frac{Pe}{z/(2R_f)}\right)^{1/3} - 1.2 - 0.28057 \cdot \left(\frac{Pe}{z/(2R_f)}\right)^{-1/3} \quad (18)$$

where *Nu* is the average Nusselt number – as denoted by Newman – referring to the concentration difference at the inlet, and *Pe* is the mass Péclet number:

$$Pe = \frac{2R_f u}{D}$$

The first term in the RHS of Eq. (18) is the zero-order solution of the constant wall temperature/concentration BC, that is, Lévêque solution with fully developed velocity profile in cylindrical coordinates [Shih and Tsou, 1978, Newman, 1967]. Notice that $(\frac{Pe}{z/(2R_f)}) = Gz$ as defined in the Introduction section; Eq. (18) is identical to the solution provided by Shih and Tsou [1978] – with one more term – with the notation of $Gz' = \pi/4 \cdot Gz$.

Remarkably, the Lévêque solution appears rounded-off to the Eq. (17) version as early as 1954 (1st edition: 1933) as directly applied to heat transfer by McAdams, [1954] (see also Shah and London [1978] and Drew et al. [1931]). The author correlated experimental data as adapted from the constant temperature BC case using a mean Nusselt number based on an arithmetic instead of a logarithmic mean temperature difference (whether arithmetic or logarithmic concentration difference is used in the corresponding correlations is also confusing) – for the definition of Gz' for heat transfer see [Shih and Tsou, 1978]:

$$Nu = 1.62 \cdot \left(\frac{4Gz'}{\pi}\right)^{1/3} = 1.62 \cdot Gz^{1/3} \quad (19)$$

Apparently, two "solutions" for the Graetz problem (constant temperature or concentration BC) exist: one applied in the entrance region (e.g. Lévêque-Newman-McAdams correlations) and one applied far from the entrance (Graetz series – Pantoleontos et al. solution [Pantoleontos et al., 2010] for very large values of Sh_W). Still, the question is: does this BC hold for membrane-based processes with a non-zero resistance in mass transport, which is imposed by the membrane itself? Shah & London illuminate the constant wall temperature BC as that "the thermal resistance of both the wall and t_a fluid [equivalent to $C_{s,z}$ in Figure 1] is zero and t_a [$C_{s,z}$] is constant" [Shah and London, 1978]; in other words, the Sh_W (and K_{ext} for that matter) are infinite, a *sine qua non* prerequisite for the Dirichlet BC to hold. Or as Kooijman articulates: "For decreasing values of the wall mass-transfer resistance the boundary condition with constant concentration at the membrane-fluid interface is approached" [Kooijman, 1973]. Or more recently, as Mi & Hwang reckon about the Lévêque correlation: "the boundary condition of constant wall concentration may not always prevail in membrane systems" [Mi and Hwang, 1999].

These passages have escaped the attention of the corresponding authors [Rongwong et al., 2012, Atchariyawut et al., 2007, Lu et al., 2008, Lin et al., 2009, Mansourizadeh and Ismail, 2009, Portugal et al., 2009, Rongwong et al., 2009, Rongwong et al., 2013, Rongwong et al., 2015, Scholes et al., 2012, Cui et al., 2015, Boributh et al., 2011, Boributh et al., 2013, Rahbari-Sisakht et al., 2012, Wang et al., 2013, Iliuta et al., 2015, Jin et al., 2017, Li et al., 2017, Ghobadi et al., 2018, Nakhjiri et al., 2018, Xu et al., 2019, Lee et al., 2020, Nakhjiri and Heydarinasab, 2020, Cao et al., 2020] and reviewers altogether. The implications of using the Lévêque-McAdams correlation without testing the hypothesis of no mass transfer resistance are, simply and tautologically, that the membrane and the shell-side (boundary layer) resistances are irrelevant, as they are assumed to be zero (obviously, if the combined membrane and shell-side resistance is zero, then both, membrane and shell-side resistances, are also zero as Eq. (6) indicates, since they are non-negative); or, if the calculated mass transport resistances are not very small, the Lévêque correlations do not hold.

The above analysis has further connotations: since there is no resistance in the membrane-wall *whatsoever* (again, when considering the Graetz-Lévêque formulation), any limiting parameter in the membrane slowing down mass transfer, such as wetting [Rongwong et al., 2012, Atchariyawut et al., 2007, Lu et al., 2008, Lin et al., 2009, Rongwong et al., 2009, Rongwong et al., 2013, Rongwong et al., 2015, Scholes et al., 2012, Cui et al., 2015, Boributh et al., 2011, Boributh et al., 2013, Rahbari-Sisakht et al., 2012, Wang et al., 2013, Cao et al., 2020], is inconsistent with the Graetz problem prerequisites, and obviously, with the Lévêque correlations application. The latter observation has been also put forward by Malek et al. in their seminal paper regarding membrane wetting [Malek et al., 1997].

Another critical point rejecting the application of the Lévêque correlation is its validity only for small $\hat{z}$-values. Wang et al. [2017] report that the Lévêque solution clearly overestimates experimental Sherwood data within the low Graetz range ($Gz<10$), that is, for $\hat{z}>0.1$ [Wang et al., 2017] and references mentioned therein. The authors found that for $\hat{z}<0.5$ the Newman solution, Eq. (18), is better suited instead of the Lévêque correlation, Eq. (17). For commercial membrane modules, when the gas mixture is within the lumen side the lowest $\hat{z}$ achievable may be around 300. Pantoleontos et al. used a commercial

1 × 5.5 Mini-Module (MM) with a gaseous lumen volumetric flowrate of ~340 cm^3/min (the highest recommended by the company is 500 cm^3/min for this type of module) yielding $\hat{z}$=39.45 [Pantoleontos et al., 2017], which is far beyond the application of the Lévêque-Newman-McAdams correlations. Note that in gas-liquid contact membrane processes (gas in the lumen) the higher the $\hat{z}$-value (the smaller the Gz number), the higher the removal efficiency of the gaseous component of interest [Pantoleontos et al., 2017, Gomez-Coma et al., 2016].

Nevertheless, "entrance-region" analysis (high Graetz number values: application of the Lévêque-Newman-McAdams correlations) is suitable for microchannels [Lopes et al., 2012], such as electrochemical microreactors, in which $\hat{z}$ could get a value of 3.8×10^{-3} [Yoon et al., 2006] – still, checking the validity of the no-wall-resistance assumption is imperative. High Gz values can be achieved in the gas-liquid contact membrane processes when the liquid flows in the lumen side since the gaseous mixture diffusivity through liquids is several orders of magnitude smaller than that of the gas-gas diffusivity. For example, in a 1 × 5.5 MM Aligwe et al. calculated that Gz numbers may well exceed 400 in experiments with NH_4Cl solution fed in the lumen side [Aligwe et al., 2019]. Note that for reactive cases in the lumen side a reaction rate term has to be added in Eq. (1), a fact also neglected by the corresponding authors [Rongwong et al., 2012, Atchariyawut et al., 2007, Lu et al., 2008, Rongwong et al., 2009, Rongwong et al., 2013, Rongwong et al., 2015, Cui et al., 2015, Boributh et al., 2013, Wang et al., 2013]: another departure from the Graetz problem as described by Graetz – see also discussion in Kumar et al. [2002] about theoretical aspects in the presence of reaction.

For gas-liquid processes and liquid in the lumen side Wickramasinghe et al. [Wickramasinghe et al., 1992] and Li & Chen [Li and Chen, 2005] suggest that the Lévêque-Newman solutions may be applicable for physical absorption cases at high Gz numbers. The rationale of this approach lies not on the absence of the membrane and shell-side resistances (which are still not zero), but in the relatively higher lumen resistance due to physical absorption compared to the other mass transfer resistances – see also Reed et al. [Reed et al., 1995] with examples covering other membrane processes.

3. Results and discussion

3.1. Analytical solution

The set of Eqs. (8)-(11) can be solved analytically by the separation of variables method, which yields an infinite series solution [Pantoleontos et al., 2010]:

$$\hat{C}(\hat{z},\hat{r}) = \sum_{n=1}^{\infty} c_n \cdot R(\hat{r}) \cdot exp\left(-2 \cdot \Lambda_n^2 \cdot \hat{z}\right) \tag{20}$$

where

$$R(\hat{r}) = M\left(\frac{1}{2} - \frac{\Lambda_n}{4}, 1, \Lambda_n \cdot \hat{r}^2\right) \cdot exp\left(-\frac{\Lambda_n \cdot \hat{r}^2}{2}\right) \tag{21}$$

$$c_n = \frac{\int_0^1 \hat{r} \cdot \left(1-\hat{r}^2\right) \cdot R(\hat{r}) d\hat{r}}{\int_0^1 \hat{r} \cdot \left(1-\hat{r}^2\right) \cdot R^2(\hat{r}) d\hat{r}} \tag{22}$$

For every Sh_W the eigenvalues, Λ_n, are the zeros of the equation:

$$\left(\frac{Sh_W}{2} - \Lambda_n\right) \cdot M\left(\frac{1}{2} - \frac{\Lambda_n}{4}, 1, \Lambda_n\right) + 2 \cdot \Lambda_n \cdot \left(\frac{1}{2} - \frac{\Lambda_n}{4}\right) \cdot M\left(\frac{3}{2} - \frac{\Lambda_n}{4}, 2, \Lambda_n\right) = 0 \tag{23}$$

The open-source mathematics software SageMath can identify the eigenvalues, Λ_n, and the Fourier coefficients, c_n, along with the mixed-cup concentration (see Supplementary Material – Appendix A, Table S1). The first step is to define Sh_w – as described in Section 2 – and then the number of the desired eigenvalues, n (nu_eigen). In addition, suppose that one would like to find the concentrations for $\hat{z}$=0.0001 (z_wanted): for the Λ_n values found, the Fourier coefficients are calculated as the ratio of two integrals as in Eq. (22), and these values are substituted in the series Eq. (20). The symbol M in Eqs. (21),(23) is the Kummer function, which in the SageMath software is denoted as the library routine, *hypergeometric_M*. For further information about derivation of the analytical solution the reader is referenced to Pantoleontos et al. [2010].

Table 2 presents various literature values of $Sh_{avg,z}$ and Sh_z for the two extreme cases of $Sh_W=\infty$ (Graetz problem) and $Sh_W=0$ compared with the values derived in the current study using the infinite series solution by Pantoleontos [Pantoleontos et al., 2010] with the aid of SageMath [code in Supplementary Material – Appendix A, Table S1; $Sh_W=10^8$ (resembling infinity) and $Sh_W=10^{-6}$ (resembling zero)] in Jupyter Notebook [Jupyter, 2021]. It is shown that the infinite series solution is valid and accessible for all Sh_W values using 128 eigenvalues in SageMath for $\hat{z} \geq 0.000025$, that is, virtually for every case of interest covering the whole $\hat{z}$-domain, from the entrance region to much bigger values of $\hat{z}$. Derivation of the first eleven eigenvalues ("L" in SageMath notation) for $Sh_W=10^8$ reveals that these are the same with those derived by Brown [1960], who solved the Graetz problem with constant tube wall temperature (Dirichlet BC). All calculations in Supplementary Material – Appendix A, Table S1 code need less than a minute to perform in an Intel® Core™ i5-4460 3.20 GHz processor.

It has to be noted that for $Sh_W=10^8$ and $\hat{z} > 50$ SageMath cannot derive the local lumen Sherwood numbers as it encounters a singularity: the mixed-cup concentration – the actual variable of interest for the researcher – is virtually zero from $\hat{z} = 1$ already, since its value is lower than 5×10^{-7} (no units).

3.2. Numerical solution – extension to nonlinear BCs

The set of Eqs. (8)-(11) is sometimes inadequate to describe all computational zones of different compartments of a membrane system, since mass balance in the shell side is also essential, especially when reactive terms are added or the shell-side concentration varies with the length. In these cases a numerical solution is called for.

As suggested by Pantoleontos et al. [2010]; Pantoleontos et al. [2017 the system of Eqs. (8)-(11) can be treated in a method-of-lines approach by discretizing the spatial derivatives (r-domain) using algebraic approximations, except for the initial value variable (z-domain), so that the system after discretization comprises a system of *n* initial-value ordinary differential equations (ODE) with respect to z, where *n* is the number of the discretization node points in the r-domain. Discretization in both z and r (or $\hat{z}$ and $\hat{r}$) directions is unavoidable if dynamic variation is considered, or axial dispersion terms (2^{nd} order derivatives) are important comprising the extended Graetz problem (see e.g. a recent study by Sohaib et al. [2021]), or a boundary-value problem with respect to $\hat{z}$ emerges, e.g. a counter-current mode of operation in the lumen-shell compartments.

In all cases considered above discretization with respect to $\hat{r}$ is necessary: afterwards, the resulted system of ODEs can be numerically solved by Runge-Kutta-like algorithms or Gear method for stiff problems [Pantoleontos et al., 2010], or it can be even solved semi-analytically (for linear lumen-wall BCs, or for BCs that can be solved for the dependent variable) [Haran and White, 1996, Subramanian and White, 2004, Ali and Saleem, 2017] – see Supplementary Material – Appendix B; likewise, this system can be further discretized with respect to $\hat{z}$ for all other reasons mentioned above.

The dimensionless PDE set (8)-(11) has two independent variables, the time-like non-negative $\hat{z}$ and the radial dimensionless $\hat{r}$ which is bounded between 0 and 1. This is convenient because the discretization points lying in the range {0,1} can be chosen as the roots of the Jacobi polynomials which are orthogonal with respect to the weighting function $r^{\beta}(1-r)^{a}$ [Rice and Do, 2012]. The Jacobi polynomials of N-th degree, $J_N^{\alpha,\beta}$, are explicitly given by the Rodrigues formula

Table 2
Comparison of values of Sh_z and $Sh_{avg,z}$ derived by different methods.

	$Sh_W=\infty$							$Sh_W=0$		
$\hat{z}$	Sh_z [a]	Sh_z [b]	Sh_z [c]	$Sh_{avg,z}$ [b]	$Nu_{avg,z}$ [d]	$Nu_{avg,z}$ [e]	$Sh_{avg,z}$ [c]	Sh_z [a]	Sh_z [b]	Sh_z [c]
1.0×10^{-6}			85.0929		162.109	160.358	182.9111			114.0186
1.0×10^{-5}			48.8851		74.655	73.869	73.8319			59.5206
2.5×10^{-5}	35.806	35.805	35.8059	54.176			54.1732	43.651	43.654	43.6614
5.0×10^{-5}	28.254	28.254	28.2536	42.814			42.8126	34.511	34.510	34.5176
1.0×10^{-4}	22.278	22.280	22.2785	33.811	34.175	33.815	33.8103	27.276	27.275	27.2757
2.0×10^{-4}		17.559	17.5595	26.684			26.6833		21.557	21.5575
2.5×10^{-4}	16.264	16.264	16.2640	24.723			24.7226	19.987	19.987	19.9868
4.0×10^{-4}		13.842	13.8421	21.049			21.0488		17.049	17.0486
5.0×10^{-4}	12.824	12.824	12.8242	19.501			19.5005	15.813	15.814	15.8127
7.0×10^{-4}		11.433	11.4332	17.739			17.3792		14.123	14.1228
1.0×10^{-3}	10.130	10.131	10.1302	15.384	*15.539	*15.384	15.3842	12.538	12.539	12.5382
2.0×10^{-3}		8.0363	8.0362	12.152			12.1515		9.9864	9.9863
2.5×10^{-3}	7.470	7.4704	7.4704	11.269			11.2690	9.295	9.2951	9.2950
4.0×10^{-3}		6.4296	6.4296	9.6281			9.6280		8.8020	8.0200
5.0×10^{-3}	6.002	6.0015	6.0015	8.9433	*9.0442	*8.9432	8.9432	7.494	7.4937	7.4937
7.0×10^{-3}		5.4301	5.4301	8.0145			8.0145		6.7881	6.7881
1.0×10^{-2}	4.917	4.9161	4.9161	7.1553	*7.2411	*7.1552	7.1552	6.149	6.1482	6.1481
2.0×10^{-2}		4.1724	4.1724	5.8147			5.8146		5.1984	5.1984
4.0×10^{-2}		3.7689	3.7689	4.8668			4.8668		4.6213	4.6213
7.0×10^{-2}		3.6688	3.6688	4.3674			4.3674		4.4162	4.4162
1.0×10^{-1}		3.6581	3.6581	4.1556	4.2309	4.1556	4.1556		4.3748	4.3748
2.0×10^{-1}		3.6568	3.6568	3.9063	3.9063	3.9063	3.9063		4.3637	4.3637
4.0×10^{-1}		3.6568	3.6568	3.7816			3.7815		4.3636	4.3636
7.0×10^{-1}		3.6568	3.6568	3.7281			3.7281		4.3636	4.3636
1		3.6568	3.6568	3.7067			3.7067		4.3636	4.3636
2		3.6568	3.6568	3.6804			3.6817		4.3636	4.3636

[a] entrance region solution – similarity transformation – Worsøe-Schmidt [1967] (as reported in Qin and Cabral [1997])
[b] orthogonal collocation on finite elements – [Qin and Cabral, 1997]
[c] separation of variables – current study – 128 eigenvalues – implementation of Supplementary Material – Appendix A, Table S1; for $Sh_W=10^8$ (∞) and $Sh_W=10^{-6}$ (0)
[d] coupling of separation of variables and method of lines – Salazar et al. [1988]
[e] Graetz series – Lévêque series (entrance region) – Shah [1975] (as reported in [Salazar et al., 1988])
* These values were originally taken (and most probably mislabelled) for $\hat{z}=5.0\times10^{-3}$, 1.0×10^{-2}, 5.0×10^{-2}, respectively [Salazar et al., 1988].

[Pantoleontos et al., 2010, Rice and Do, 2012]:

$$J_N^{\alpha,\beta}(r)\left[r^{\beta}(1-r)^{a}\right]=\frac{(-1)^N\Gamma(\beta+1)}{\Gamma(N+\beta+1)}\frac{d^N}{dr^N}\left[r^{N+\beta}(1-r)^{N+a}\right] \tag{24}$$

where Γ is the gamma function. An important note is that since there are two boundary conditions with respect to r, both end points ($\hat{r}_1=0$, $\hat{r}_{N+2}=1$) are included in the overall evaluation, so that the N interior collocation points are zeros of the Jacobi polynomial $J_N^{\alpha+1,\beta+1}$ rather than $J_N^{\alpha,\beta}$ [87].

Following Rice and Do, for N interior node points plus the boundary points 0 and 1, the N+2 degree (node) polynomial is defined as [Rice and Do, 2012]:

$$p_{N+2}(\hat{r})=\prod_{j=1}^{N+2}\left(\hat{r}-\hat{r}_j\right)=\hat{r}(\hat{r}-1)\prod_{j=2}^{N+1}\left(\hat{r}-\hat{r}_j\right) \tag{25}$$

The derivatives at the point *i* are given by [Rice and Do, 2012]:

$$\frac{\partial\hat{C}_i}{\partial\hat{r}_i}=\sum_{j=1}^{N+2}A_{i,j}\hat{C}_j,\ \frac{\partial^2\hat{C}_i}{\partial\hat{r}_i^2}=\sum_{j=1}^{N+2}B_{i,j}\hat{C}_j \tag{26}$$

where the elements of the square matrices (N+2, N+2) $A_{i,j}$ and $B_{i,j}$ are defined as [Rice and Do, 2012]:

$$A_{i,j}=\begin{cases}\frac{p_{N+2}^{(2)}(\hat{r}_i)}{2p_{N+2}^{(1)}(\hat{r}_i)} & for\ j=i\\ \frac{p_{N+2}^{(1)}(\hat{r}_i)}{(\hat{r}_i-\hat{r}_j)p_{N+2}^{(1)}(\hat{r}_j)} & for\ j\neq i\end{cases},\ B_{i,j}=\begin{cases}\frac{p_{N+2}^{(3)}(\hat{r}_i)}{3p_{N+2}^{(1)}(\hat{r}_i)} & for\ j=i\\ 2A_{i,j}\left(A_{i,i}-\frac{1}{\hat{r}_i-\hat{r}_j}\right) & for\ j\neq i\end{cases} \tag{27}$$

where $p_{N+2}^{(k)}(\hat{r}_i)$ is the k-th derivative of the node polynomial at point $\hat{r}_i$.

Including both end points comprises the Gauss-Lobatto quadrature [Rice and Do, 2012] (necessary for the evaluation of the integral of the dimensionless mixed-cup concentration). Let $a'=a+1$, $\beta'=\beta+1$. The Lobatto weights are calculated by the following formula [Rice and Do, 2012]:

$$\begin{aligned}w_i&=\frac{\left(2N+\alpha'+\beta'+1\right)c_N^{(\alpha',\beta')}}{\left[p_{N+2}^{(1)}(\hat{r}_i)\right]^2}\cdot K_i,\ K_i=\begin{cases}\frac{1}{\beta'}\ for\ i=1\\ 1\ for\ i=2..N+1\\ \frac{1}{a'}\ for\ i=N+2\end{cases},\ c_N^{(\alpha',\beta')}\\ &=\frac{\mathrm{N!}}{\gamma^2(2N+a'+\beta'+1)}\frac{\Gamma^2\left(\beta'+1\right)\cdot\Gamma\left(N+a'+1\right)}{\Gamma(N+\beta'+1)\cdot\Gamma(N+a'+\beta'+1)},\ \gamma\\ &=\frac{\Gamma\left(2\mathrm{N}+\alpha'+\beta'+1\right)\cdot\Gamma\left(\beta'+1\right)}{\Gamma(\mathrm{N}+\alpha'+\beta'+1)\cdot\Gamma(\mathrm{N}+\beta'+1)}\end{aligned} \tag{28}$$

The set of Eqs. (24)-(28) is the orthogonal collocation method using the Jacobi polynomials for the discretization of the first and second derivative of any function defined in the domain {0,1}, the determination of the collocation matrices and the Gauss-Lobatto weights. SageMath may identify the roots, weights and matrices of the collocation method as demonstrated in Supplementary Material – Appendix A, Table S2; indicative calculated values are presented inTable 3.

Since there is already an efficient and practical analytical solution expressed in Eqs. (20)-(23) (see Supplementary Material – Appendix A, Table S1), a numerical solution of the set of Eqs. (8)-(11) is no longer pursued; instead, an extension to the original problem by including a nonlinear wall-BC is attempted. Nevertheless, a semi-analytical treatment of Eqs. (8)-(11) is also presented in Supplementary Material – Appendix B most suited for linear problems for which analytical solutions are not available.

A set of nonlinear BCs accounting for supported liquid membrane, facilitated transport, membrane extraction and other membrane-based processes is handily available in the invaluable work by Qin and

Table 3
Indicative values of the Gauss-Jacobi-Lobatto quadrature points, weights and $A_{i,j}$, $B_{i,j}$ matrices.

$\alpha' = \beta' = 2$	N = 4	N = 5	N = 6	N = 7	N = 8
$\hat{r}_j$ (j=1..N+2)	0	0	0	0	0
	0.152627	0.115272	0.090077	0.072299	0.059296
	0.374719	0.289543	0.229698	0.186311	0.153970
	0.625281	0.500000	0.405661	0.334185	0.279284
	0.847373	0.710457	0.594339	0.500000	0.424184
	1	0.884728	0.770302	0.665815	0.575816
		1	0.909923	0.813689	0.720716
			1	0.927701	0.846030
				1	0.940704
					1
w_j (j=1..N+2)	0.001190	0.000661	0.000397	0.000253	0.000168
	0.024576	0.014842	0.009407	0.006218	0.004261
	0.057567	0.040740	0.028558	0.020212	0.014541
	0.057567	0.054180	0.044972	0.035542	0.027604
	0.024576	0.040740	0.044972	0.042218	0.036760
	0.001190	0.014842	0.028558	0.035542	0.036760
		0.000661	0.009407	0.020212	0.027604
			0.000397	0.006218	0.014541
				0.000253	0.004261
					0.000168
$A_{i,j}$ (N = 4; $\alpha' = \beta' = 2$)					
-13.000000	21.049759	-13.122203	7.863873	-3.791429	1.000000
-2.039350	-2.685908	6.891308	-3.238101	1.439374	-0.367323
0.542729	-2.941934	-0.534695	3.991015	-1.382362	0.325246
-0.325246	1.382362	-3.991015	0.534695	2.941934	-0.542729
0.367323	-1.439374	3.238101	-6.891308	2.685908	2.039350
-1.000000	3.791429	-7.863873	13.122203	-21.049759	13.000000
$B_{i,j}$ (N = 4; $\alpha' = \beta' = 2$)					
114.000000	-271.460495	271.139647	-179.307633	89.628481	-24.000000
37.678388	-63.928203	25.039330	3.692721	-3.588457	1.106222
-3.477115	29.639017	-50.071797	27.588457	-4.371068	0.692505
0.692505	-4.371068	27.588457	-50.071797	29.639017	-3.477115
1.106222	-3.588457	3.692721	25.039330	-63.928203	37.678388
-24.000000	89.628481	-179.307633	271.139647	-271.460495	114.000000

Table 4
Dimensionless lumen-wall BCs and reference cases [Qin and Cabral, 1998].

Type	Dimensionless gradient at $\hat{r} = 1$		Reference values
1	$-\frac{Sh_W}{2}(1 + a_1 \cdot \hat{C}(\hat{z},1))\hat{C}(\hat{z},1)$	(29)	$Sh_W = 5$; $a_1 = 19$
2	$-\frac{Sh_W}{2}\frac{\hat{C}(\hat{z},1)}{1+a_2\cdot\hat{C}(\hat{z},1)}$	(30)	$Sh_W = 1000$; $a_2 = 100$
3[a]	$-\frac{Sh_W}{2}\frac{\hat{C}^2(\hat{z},1)}{1+a_3\cdot\hat{C}^2(\hat{z},1)}$	(31)	$Sh_W = 100$; $a_3 = 9$
4[b]	$-\frac{Sh_W}{2}\frac{\hat{C}(\hat{z},1)}{1+a_4\cdot\hat{C}(\hat{z},1)+\sqrt{1+2a_4\cdot\hat{C}(\hat{z},1)}}$	(32)	$Sh_W = 100$; $a_4 = 9$

[a] typographical error in the main table of the original manuscript [Qin and Cabral, 1998] – a minus (-) sign instead of the correct (+) in the denominator

[b] probably mislabelled as Sh_W=50 instead of 100 in the original manuscript [Qin and Cabral, 1998]

Cabral, [1998] as summarized in Table 4 (with literature reference values for computational purposes). For the derivation of each BC and the actual variation range of the parameters the reader is referenced to Qin and Cabral [1998]. For nonlinear lumen-wall BCs the resulted nonlinear algebraic equation after discretization cannot be directly solved for $\hat{C}_{N+2}$ (see Supplementary Material – Appendix B for the linear case) – where $\hat{C}(\hat{z},1) = \hat{C}_{N+2}$ – giving rise to an initial-value (IV) differential-algebraic (DAE) system – with *algebraic* signifying a dependent variable without its derivative.

The solvers most frequently used for IV-DAE systems are extensions of standard numerical methods designed for IV-ODEs, but with one crucial prerequisite: a consistent set of initial conditions with respect to the DAE satisfying all constraints and variables is expected by the solver – in ODE-cases the *consistency* is not a prerequisite for the algorithm. In either case, DAEs or ODEs, a root-finding procedure is incorporated assigning consistent initial conditions to all dependent variables for successful and accurate differentiation. In the following lines in order to highlight the rationale of the DAE-to-ODE adaptation all algebraic equations are manually transformed to differential equations to comprise an explicit IV-ODE system: the user's intervention ensures that an analytical function is provided as the differential equation, which would otherwise be approximated by the DAE-algorithm. Additionally, implementation of a DAE-solver is avoided and a typical ODE-solver is directly invoked.

The initial (at $\hat{z} = 0$) values of the concentrations in the interior points (referring to the discretization-$\hat{r}$-points), Eq. (S3), are given in Eq. (S4) – see Supplementary Material – Appendix B). For a nonlinear lumen-wall BC the missing initial values of the two exterior points are calculated by solving a 2 × 2 system of algebraic equations. For example, when the mass transfer problem is determined by Eq. (31) at the boundary, one has to solve the following two equations with respect to *f, g*:

$$A_{1,1}\cdot f + A_{1,N+2}\cdot g + \sum_{j=2}^{N+1} A_{1,j} = 0 \tag{33}$$

$$A_{N+2,1}\cdot f + A_{N+2,N+2}\cdot g + \sum_{j=2}^{N+1} A_{N+2,j} = -\frac{Sh_W}{2}\frac{g^2}{1+a_3\cdot g^2} \tag{34}$$

where $\hat{C}_1(0) = f$ and $\hat{C}_{N+2}(0) = g$, since $\hat{C}_i(0) = 1\ for\ i = 2..N+1$.

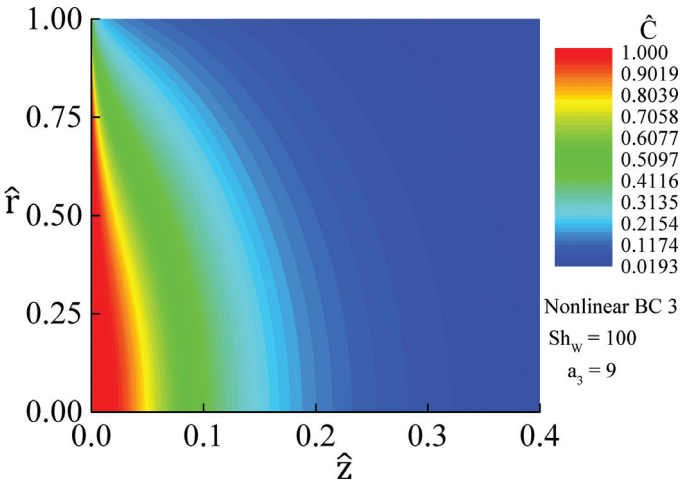

Figure 2. Contour plot of the dimensionless concentration, $\hat{C}$, with respect to axial and radial distances ($\hat{z}$, $\hat{r}$) for nonlinear BC3 (reference values: $Sh_W = 100$; $a_3 = 9$).

The remaining ODEs at the boundaries can be found by differentiating Eq. (S1) and Eq. (31) with respect to $\hat{z}$:

$$A_{1,1}\frac{d\hat{C}_1}{d\hat{z}} = -\sum_{j=2}^{N+2} A_{1,j}\frac{d\hat{C}_j}{d\hat{z}} \tag{35}$$

$$\left[A_{N+2,N+2} + \frac{Sh_W\hat{C}_{N+2}}{\left(1+a_3\cdot\hat{C}_{N+2}^2\right)^2}\right]\frac{d\hat{C}_{N+2}}{d\hat{z}} = -\sum_{j=1}^{N+1} A_{N+2,j}\frac{d\hat{C}_j}{d\hat{z}} \tag{36}$$

Applying the Gauss-Jacobi-Lobatto formulation to Eq. (12) the dimensionless mixed-cup concentration can be calculated by the following formula:

$$C_{mc}^{*}(\hat{z}) = 4\sum_{j=1}^{N+2} w_i\left(1+\hat{r}_j\right)\hat{C}_j \tag{37}$$

for $\alpha = 1$ and $\beta = 1$, and apparently $\alpha' = \beta' = 2$.

To sum up, when Eq. (31) applies, the final (N+2) × (N+2) IV-ODE system consists of the differential Eqs. (35, 36) and (S3) with initial conditions (33), (34) and (S4), respectively. SageMath can still be used to solve the system with reasonable accuracy by importing the *solve_ivp* function as demonstrated in Supplementary Material – Appendix A, Table S3 – the interested user should directly incorporate the script under the code of Supplementary Material – Appendix A, Table S2. In all SageMath implementations for the nonlinear BCs, the default IV-ODE method is invoked, namely the 'RK45' which stands for the explicit Runge-Kutta method of order 5(4). For further information the reader is referenced to the *scipy.integrate.solve_ivp* user notes [SageMath, 2021].

Figure 2 depicts the isolines (contour plot) of the dimensionless concentration, $\hat{C}$, with respect to axial ($\hat{z}$) and radial ($\hat{r}$) distances for the nonlinear BC3, Eq. (31) (reference values: $Sh_W = 100$; $a_3 = 9$). This is a typical illustration when variation in both directions is comparable, which occurs when the combined mass transfer coefficient is very large. Concentration variation is more intense in the axial compared to the radial direction; e.g. for $\hat{r}$=0.5 concentration variation is 97% between inlet-outlet ($\hat{z}$=0 to 0.4), while for $\hat{z}$=0.2 the concentration variation exceeds 68% from the symmetry point ($\hat{r}$=0) to the inner wall radius ($\hat{r}$=1), where the concentration has the lowest value due to the sink-term-BC, Eq. (31). Another observation arising from this figure is that for a certain Sh_W ($=2K_{ext}R_f/D$) the concentration decreases for larger values of $\hat{z}$ ($=zD/4uR_f^2$) entailing that the separation efficiency increases when the fiber length increases or/and the lumen fluid velocity decreases, that is, the effective time of a fluid element remaining in the lumen side increases.

In Table 5 mixed-cup concentration for various $\hat{z}$-points is presented for all BCs and the reference values of Table 4 along with the literature values by Qin and Cabral, who used the orthogonal collocation on finite elements in both directions ($\hat{z}$ and $\hat{r}$) [Qin and Cabral, 1998]. SageMath performs fairly well with satisfactory computational time (almost one hour) for 16 interior node points. However, if higher precision is needed, SageMath fails to deliver the desired values in reasonable time (e.g. for 24 interior collocation points and very small relative and absolute tolerances (*atol=rtol=1e-10* in *scipy.integrate.solve_ivp* notation) SageMath would need more than 72 hours to get past $\hat{z}$=0.1 in the i5-4460 3.20 GHz processor). While the very slow computations may be attributed to possible algorithmic inexpediency as commanded by the authors of the current study in Supplementary Material – Appendix A, Table S3, the inadequacy of the default built-in ODE-solvers and their core reliance to *Python* interpreter at every time-step during integration might also be the reason for *solve_ivp* performing poorly.

The same methodology is attempted using the commercial mathematical software [Maple, 2021.1 release], which incorporates the Modified Extended Backward Differentiation Equation Implicit (*mebdfi*) method for both DAE/ODE systems [Maple, 2021]. More details can be found in the work by Cash [2000] and in the corresponding help-pages of Maple [2021]. The benchmark test is to replicate the Sh_z values as calculated by Qin and Cabral [1998] by using Eq. (16). Figure 3 depicts the variation of Sh_z minus $Sh_z(Sh_w \to \infty \;\&\; a_i = 0)$ with $\hat{z}$ at various values of a_i for the four nonlinear BCs generated in Maple with 32 interior collocation points and invoking *dsolve/numeric/mebdfi* method with *abserr = relerr = 1e-10* (Supplementary Material – Appendix A, Table S4 presents the code for evaluating the Gauss-Jacobi-Lobatto quadrature points, weights and $A_{i,j}$, $B_{i,j}$ matrices in Maple for comparison and direct use) – again, in Maple the ODE-systems are solved as described in the previous analysis.

Comparing with Table 4 and following the analysis in Section 2.2, it can be deduced that for the cases of BC1, BC2, BC4 the value of Sh_z when $Sh_w \to \infty$ and $a_i = 0$ is equivalent to the value of Sh_z for the linear BC case when $Sh_w \to \infty$, that is, it would be the same as solving the mass transfer problem with the Dirichlet BC: $\hat{C}(\hat{z},1) = 0$. In a similar fashion, when $Sh_w \to \infty$ & $a_3 = 0$, BC3 is reduced to the BC: $\hat{C}^2(\hat{z},1) = 0 \Rightarrow \hat{C}(\hat{z},1) = 0$. Thus, for all nonlinear BCs examined in Table 4, the value of Sh_z ($Sh_w \to \infty$ & $a_i = 0$) is derived from the fourth column of Table 2. The curves of Figure 3 are identical with those by Qin and Cabral [1998] for the actual range of interest $\hat{z} \geq 10^{-4}$ and need less than 900s to be generated. The *mebdfi* method as incorporated in Maple is apparently the most suitable approach for the treatment of such problems, while performing incomparably faster than similar methods. Nevertheless, the SageMath environment provides an affordable mathematical platform with acceptable accuracy judging from the mixed-cup concentration values (the actual variable of interest) as shown in Table 5. As the SageMath community grows steadily fast the interested reader is promptly advised to combine custom-made ODE-solvers to overcome performance and speed obstacles.

4. Conclusions

In this study the mass continuity equation for fully developed laminar flow in the lumen side of a hollow-fiber membrane contactor is solved with respect to the lumen-wall BC. While much of the attention is devoted on the carbon-capture membrane-based gas absorption process, the corresponding model is extended, incorporating various linear or nonlinear BCs that account for different membrane-based processes.

This work extensively discusses the Graetz problem and the Lévêque correlation resorting to the prerequisites, their limitations and applications. It is shown that the constant wall concentration case (Dirichlet boundary condition) imposed by the Graetz-Lévêque postulations is a sub-case of the mixed Neumann-Dirichlet linear BC largely overestimating the performance of membrane contactors. When mass transfer is determined by a linear lumen-wall BC, the existing analytical solution

Table 5
Mixed-cup concentration values for 16 interior node points in SageMath and comparison with Qin and Cabral [1998].

	BC1 (29)		BC2 (30)		BC3 (31)		BC4 (32)	
$\hat{z}$	C^*_{mc} [Qin and Cabral, 1998]	C^*_{mc} -this study	C^*_{mc} [Qin and Cabral, 1998]	C^*_{mc} -this study	C^*_{mc} [Qin and Cabral, 1998]	C^*_{mc} -this study	C^*_{mc} [Qin and Cabral, 1998]	C^*_{mc} -this study
0.001	0.9577	0.95769	0.9611	0.96105	0.9693	0.96926	0.9755	0.97543
0.002	0.9313	0.93132	0.9253	0.92533	0.9453	0.94529	0.9533	0.95332
0.004	0.8897	0.88974	0.8710	0.87096	0.9059	0.90587	0.9132	0.91324
0.007	0.8400	0.83998	0.8102	0.81018	0.8577	0.85776	0.8608	0.86077
0.010	0.7982	0.79818	0.7609	0.76095	0.8170	0.81699	0.8149	0.81485
0.015	0.7389	0.73886	0.6928	0.69284	0.7588	0.75882	0.7485	0.74852
0.020	0.6879	0.68795	0.6356	0.63562	0.7087	0.70872	0.6913	0.69129
0.025	0.6429	0.64287	0.5857	0.58573	0.6643	0.66427	0.6407	0.64067
0.030	0.6022	0.60221	0.5413	0.54129	0.6241	0.62410	0.5952	0.59517
0.035	0.5651	0.56510	0.5012	0.50117	0.5874	0.58740	0.5538	0.55381
0.040	0.5310	0.53096	0.4646	0.46462	0.5536	0.55359	0.5159	0.51592
0.045	0.4994	0.49937	0.4311	0.43111	0.5222	0.52227	0.4810	0.48100
0.050	0.4700	0.47001	0.4002	0.40027	0.4931	0.49314	0.4487	0.44869
0.060	0.4171	0.41711	0.3454	0.34542	0.4406	0.44055	0.3908	0.39083
0.070	0.3708	0.37084	0.2983	0.29834	0.3944	0.39445	0.3341	0.34068
0.080	0.3302	0.33018	0.2577	0.25777	0.3538	0.35385	0.2970	0.29703
0.090	0.2944	0.29437	0.2275	0.22276	0.3180	0.31801	0.2590	0.25900
0.100	0.2627	0.26275	0.1925	0.19252	0.2863	0.28630	0.2258	0.22583
0.120	0.2101	0.21007	0.1438	0.14381	0.2333	0.23329	0.1716	0.17165
0.140	0.1687	0.16869	0.1074	0.10743	0.1915	0.19148	0.1304	0.13042
0.160	0.1360	0.13604	0.0825	0.08025	0.1583	0.15834	0.0991	0.09907
0.200	0.0895	0.08953	0.0448	0.04478	0.1108	0.11077	0.0571	0.05713
0.250	0.0541	0.05412	0.0216	0.02160	0.0740	0.07397	0.0287	0.02869
0.300	0.0333	0.03330	0.0104	0.01041	0.0517	0.05172	0.0144	0.01440
0.400	0.0131	0.01308	0.0024	0.00242	0.0286	0.02860	0.0036	0.00362

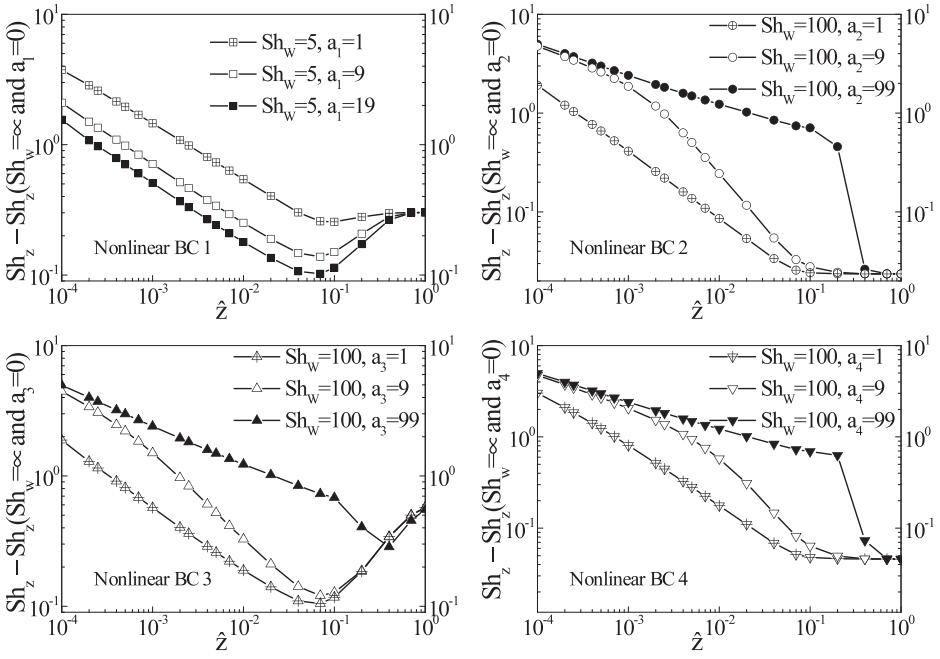

Figure 3. Variation of Sh_z minus $Sh_z(Sh_w \to \infty \ \& \ a_i = 0)$ with $\hat{z}$ at various values of a_i for the four nonlinear BCs generated in Maple with 32 interior collocation points and invoking *dsolve/numeric/mebdfi* method.

derived by the separation of variables method is proven to be very accurate and practical even in the region very close to the entrance of the computational domain avoiding the need for numerical or entrance-region solutions.

The analysis is extended solving the nonlinear lumen-wall BCs with the method-of-lines approach by discretizing the r-domain using the Gauss-Jacobi-Lobatto orthogonal collocation and integrating the resulting initial-value ordinary differential equations system. The overall treatment of the corresponding nonlinear PDEs in Maple computing platform is shown to be much superior to other approaches. Additionally, the open-source computational software SageMath can be a promising alternative, providing an affordable and competent equation-based modelling platform with unlimited capabilities of development and content.

Declaration of Competing Interest

The authors declare that they have no known competing financial interests or personal relationships that could have appeared to influence the work reported in this paper

Acknowledgments

This project has received funding from the European Union's Horizon 2020 research and innovation programme under grant agreement No 814548.

Supplementary materials

Supplementary material associated with this article can be found, in the online version, at doi:10.1016/j.ccst.2021.100027.

References

Ali, I., Saleem, M.T., 2017. A semi-analytic spectral method for elliptic partial differential equations. Electron. J. Differ. Eq. 43, 1–11.

Aligwe, P.A., Sirkar, K.K., Canlas, C.J., 2019. Hollow fiber gas membrane-based removal and recovery of ammonia from water in three different scales and types of modules. Sep. Purif. Technol. 224, 580–590.

Atchariyawut, S., Jiraratananon, R., Wang, R., 2007. Separation of CO_2 from CH_4 by using gas–liquid membrane contacting process. J. Membrane Sci. 304, 163–172.

Boributh, S., Assabumrungrat, S., Laosiripojana, N., Jiraratananon, R., 2011. Effect of membrane module arrangement of gas–liquid membrane contacting process on CO_2 absorption performance: A modeling study. J. Membrane Sci. 380, 75–86.

Boributh, S., Jiraratananon, R., Li, K., 2013. Analytical solutions for membrane wetting calculations based on log-normal and normal distribution functions for CO_2 absorption by a hollow fiber membrane contactor. J. Membrane Sci. 429, 459–472.

Bougie, F., Iliuta, I., Iliuta, M.C., 2014. Absorption of CO_2 by AHPD-Pz aqueous blend in PTFE hollow fiber membrane contactors. Sep. Purif. Technol. 138, 84–91.

Brown, G.M., 1960. Heat or mass transfer in a fluid in laminar flow in a circular or flat conduit. AIChE J 6, 179–183.

Cao, F., Gao, H., Ling, H., Huang, Y., Liang, Z., 2020. Theoretical modeling of the mass transfer performance of CO_2 absorption into DEAB solution in hollow fiber membrane contactor. J. Membrane Sci. 593, 117439.

Cao, Y., Khan, A., Nakhjiri, A.T., Albadarin, A.B., Kurniawan, T.A., Rezakazemi, M., 2021. Recent advancements in molecular separation of gases using microporous membrane systems: A comprehensive review on the applied liquid absorbents. J. Mol. Liq. 337, 116439.

Cash, J.R., 2000. Modified extended backward differentiation formulae for the numerical solution of stiff initial value problems in ODEs and DAEs. J. Comput. Appl. Math. 125, 117–130.

Churchill, S.W., 2000. The art of correlation. Ind. Eng. Chem. Res. 39, 1850–1877.

Churchill, S.W., 2013. An evaluation of the usual simplifying assumptions. Ind. Eng. Chem. Res. 52, 230–257.

Cooney, D.O., Kim, S.-S., Davis, E.J., 1974. Analyses of mass transfer in hemodialyzers for laminar blood flow and homogeneous dialysate. Chem. Eng. Sci. 29, 1731–1738.

Cui, L., Ding, Z., Liu, L., Li, Y., 2015. Modelling and experimental study of membrane wetting in microporous hollow fiber membrane contactors. Can. J. Chem. Eng. 93, 1254–1265.

Dindore, V.Y., Versteeg, G.F., 2005. Gas-liquid mass transfer in a cross-flow hollow fiber module: Analytical model and experimental validation. Int. J. Heat Mass Transfer 48, 3352–3362.

Dindore, V.Y., Brilman, D.W.F., Geuzebroek, F.H., Versteeg, G.F., 2004. Membrane-solvent selection for CO_2 removal using membrane gas-liquid contactors. Sep. Purif. Technol. 40, 133–145.

Dindore, V.Y., Brilman, D.W.F., Feron, P.H.M., Versteeg, G.F., 2004. CO_2 absorption at elevated pressures using a hollow fiber membrane contactor. J. Membrane Sci. 235, 99–109.

Dindore, V.Y., Brilman, D.W.F., Versteeg, G.F., 2005. Modelling of cross-flow membrane contactors: physical mass transfer processes. J. Membrane Sci. 251, 209–222.

Drew, T.B., Hogan, J.J., McAdams, W.H., 1931. Heat transfer in stream-line flow. Ind. Eng. Chem. 23, 936–945.

Gabelman, A., Hwang, S.-T., 1999. Hollow fiber membrane contactors. J. Membrane Sci. 159, 61–106.

Gabelman, A., Hwang, S.-T., 2006. A theoretical study of dense gas extraction using a hollow fiber membrane contactor. J. Supercrit. Fluid. 37, 157–172.

Ghiaasiaan, S.M., 2011. Convective heat and mass transfer. Cambridge University Press.

Ghobadi, J., Ramirez, D., Jerman, R., Crane, M., Khoramfar, S., 2018. CO_2 separation performance of different diameter polytetrafluoroethylene hollow fiber membranes using gas-liquid membrane contacting system. J. Membrane Sci. 549, 75–83.

Glasgow, L.A., 2010. Transport phenomena. An introduction to advanced topics. John Wiley & Sons Inc.

Gomez-Coma, L., Garea, A., Irabien, A., 2016. Carbon dioxide capture by [emim][Ac] ionic liquid in a polysulfone hollow fiber contactor. Int. J. Greenh. Gas Con. 52, 401–409.

Gustafson, K., Abe, T., 1998. The third boundary condition – was it Robin's? Math. Intell. 20, 63–71.

Haran, B.S., White, R.E., 1996. A semianalytical technique for solving nonlinear partial differential equations. Comput. Appl. Eng. Educ. 4, 229–240.

Houlker, S., Davey, C.J., Allemand, A., Brookes, A., Moore, A., Vale, P., Pidou, M., McAdam, E.J., 2021. Reconciliation of gas to liquid mass transfer in parallel and transverse flow (cross-flow) hollow fiber membrane contactors (HFMC) for CO_2 absorption. Sep. Sci. Tech. 56, 129–140.

Iliuta, I., Bougie, F., Iliuta, M.C., 2015. CO_2 removal by single and mixed amines in a hollow-fiber membrane module – investigation of contactor performance. AIChE J 61, 955–971.

Jin, P., Huang, C., Shen, Y., Zhan, X., Hu, X., Wang, L., Wang, L., 2017. Simultaneous separation of H_2S and CO_2 from biogas by gas-liquid membrane contactor using single and mixed absorbents. Energy Fuels 31, 11117–11126.

Kays, W.M., Crawford, M.E., 1993. Convective heat and mass transfer, 3rd Ed. McGraw-Hill.

Kim, J-I., Stroeve, P., 1988. Mass transfer in separation devices with reactive hollow fibers. Chem. Eng. Sci. 43, 247–257.

Knudsen, J.G., Katz, D.L., 1958. Fluid dynamics and heat transfer. McGraw-Hill, New York.

Kooijman, J.M., 1973. Laminar heat or mass transfer in rectangular channels and in cylindrical tubes for fully developed flow: comparison of solutions obtained for various boundary conditions. Chem. Eng. Sci. 28, 1149–1160.

Koutsonikolas, D.E., Pantoleontos, G., Karagiannakis, G., Konstandopoulos, A.G., 2021. Development of H_2 selective silica membranes: Performance evaluation through single gas permeation and gas separation tests. Sep. Purif. Technol. 264, 118432.

Kreulen, H., Smolders, C.A., Versteeg, G.F., van Swaaij, W.P.M., 1993. Microporous hollow fibre membrane modules as gas-liquid contactors. Part 1. Physical mass transfer processes. A specific application: Mass transfer in highly viscous liquids. J. Membrane Sci. 78, 197–216.

Kumar, P.S., Hogendoorn, J.A., Feron, P.H.M., Versteeg, G.F., 2002. New absorption liquids for the removal of CO_2 from dilute gas streams using membrane contactors. Chem. Eng. Sci. 57, 1639–1651.

Kumar, P.S., Hogendoorn, J.A., Feron, P.H.M., Versteeg, G.F., 2003. Approximate solution to predict the enhacement factor for the reactive absorption of a gas in a liquid flowing through a microporous membrane hollow fiber. J. Membrane Sci. 213, 231–245.

Lee, H.J., Kim, M.K., Park, J.H., 2020. Decompression stripping of carbon dioxide from rich monoethanolamine through porous hydrophobic modified ceramic hollow fiber membrane contactor. Sep. Purif. Technol. 236, 116304.

Li, J.-J., Chen, B.-H., 2005. Review of CO_2 absorption using chemical solvents in hollow fiber membrane contactors. Sep. Purif. Technol. 41, 109–122.

Li, Y., Wang, L., Jin, P., Song, X., Zhan, X., 2017. Removal of carbon dioxide from pressurized landfill gas by physical absorbents using a hollow fiber membrane contactor. Chem. Eng. Process. 121, 149–161.

Lin, S.-H., Tung, K.-L., Chen, W.-J., Chang, H.-W., 2009. Absorption of carbon dioxide by mixed piperazine-alkanolamine absorbent in a plasma-modified polypropylene hollow fiber contactor. J. Membrane Sci. 333, 30–37.

Lopes, J.P., Cardoso, S.S.S., Rodrigues, A.E., 2012. Bridging the gap between Graetz's and Lévêque's analyses for mass/heat transfer in a channel with uniform concentration or flux at the wall. AIChE J 58, 1880–1992.

Lu, J.-G., Zheng, Y.-F., Cheng, M.-D., Wang, L.-J., 2008. Wetting mechanism in mass transfer process of hydrophobic membrane gas absorption. J. Membrane Sci. 308, 180–190.

Mahmud, H., Kumar, A., Narbaitz, R.M., Matsuura, T., 2000. A study of mass transfer in the membrane air-stripping process using microporous polyproplylene hollow fibers. J. Membrane Sci. 179, 29–41.

Malek, A., Li, K., Teo, W.K., 1997. Modeling of microporous hollow fiber membrane modules operated under partially wetted conditions. Ind. Eng. Chem. Res. 36, 784–793.

Mansourizadeh, A., Ismail, A.F., 2009. Hollow fiber gas–liquid membrane contactors for acid gas capture: A review. J. Hazard. Mater. 171, 38–53.

Maple computing platform, 2021.1 release, https://www.maplesoft.com/products/Maple/

Mavroudi, M., Kaldis, S.P., Sakellaropoulos, G.P., 2003. Reduction of CO_2 emissions by a membrane contacting process. Fuel 82, 2153–2159.

McAdams, W.H., 1954. Heat transmission, 3rd Edition McGraw-Hill.

Mi, L., Hwang, S.-T., 1999. Correlation of concentration polarization and hydrodynamic parameters in hollow fiber modules. J. Membrane Sci. 159, 143–165.

Nakhjiri, A.T., Heydarinasab, A., 2020. Efficiency evaluation of novel liquid potassium lysinate chemical solution for CO_2 molecular removal inside the hollow fiber membrane contactor: Comprehensive modeling and CFD simulation. J. Mol. Liq. 297, 111561.

Nakhjiri, A.T., Heydarinasab, A., Bakhtiari, O., Mohammadi, T., 2018. Experimental investigation and mathematical modeling of CO_2 sequestration from CO_2/CH_4 gaseous mixture using MEA and TEA aqueous absorbents through polypropylene hollow fiber membrane contactor. J. Membrane Sci. 565, 1–13.

Newman, J., June 1967. Extension of the Lévêque solution. University of California, Ernest O. Lawrence Radiation Laboratory.

Pantoleontos, G., Kaldis, S.P., Koutsonikolas, D., Grammelis, P., Sakellaropoulos, G.P., 2010. CO_2 absorption in a mini-module membrane contactor included in. In: Dincer, I., Hepbasli, A., Midilli, A., Karakoc, T.H. (Eds.), Global Warming. Springer Science+Business Media, LLC, pp. 307–313.

Pantoleontos, G., Kaldis, S.P., Koutsonikolas, D., Skodras, G., Sakellaropoulos, G.P., 2010. Analytical and numerical solutions of the mass continuity equation in the lumen side of a hollow-fiber membrane contactor with linear or nonlinear boundary conditions. Chem. Eng. Commun. 197, 709–732.

Pantoleontos, G., Theodoridis, T., Mavroudi, M., Kikkinides, E.S., Koutsonikolas, D., Kaldis, S.P., Pagana, A.E., 2017. Modelling, simulation, and membrane wetting estimation in gas-liquid contacting processes. Can. J. Chem. Eng. 95, 1352–1363.

Portugal, A.F., Magalhães, F.D., Mendes, A., 2009. Carbon dioxide removal from anaesthetic gas circuits using hollow fiber membrane contactors with amino acid salt solutions. J. Membrane Sci. 339, 275–286.

Project Jupyter, 2021, https://jupyter.org/index.html

Qin, Y., Cabral, J.M.S., 1997. Lumen mass transfer in hollow-fiber membrane processes with constant external resistances. AIChE J 43, 1975–1988.

Qin, Y., Cabral, J.M.S., 1998. Lumen mass transfer in hollow-fiber membrane processes with nonlinear boundary conditions. AIChE J 44, 836–848.

Qin, Y., Cabral, J.M.S., Wang, S., 1996. Hollow-fiber gas-membrane process for removal of NH_3 from solution of NH_3 and CO_2. AIChE J 42, 1945–1956.

Rahbari-Sisakht, M., Ismail, A.F., Rana, D., Matsuura, T., 2012. Effect of different additives on the physical and chemical CO_2 absorption in polyetherimide hollow fiber membrane contactor system. Sep. Purif. Technol. 98, 472–480.

Reed, B.W., Semmens, M.J., Cussler, E.L., 1995. Membrane contactors, included in. In: Noble, R.D., Stern, S.A. (Eds.), Membrane separations technology. Principles and applications. Elsevier Science B.V., pp. 467–498.

Rice, R.G., Do, D.D., 2012. Applied Mathematics and Modeling for Chemical Engineers, 2nd Ed. John Wiley & Sons.

Rongwong, W., Jiraratananon, R., Atchariyawut, S., 2009. Experimental study on membrane wetting in gas–liquid membrane contacting process for CO_2 absorption by single and mixed absorbents. Sep. Purif. Technol. 69, 118–125.
Rongwong, W., Boributh, S., Assabumrungrat, S., Laosiripojana, N., Jiraratananon, R., 2012. Simultaneous absorption of CO_2 and H_2S from biogas by capillary membrane contactor. J. Membrane Sci. 392-393, 38–47.
Rongwong, W., Assabumrungrat, S., Jiraratananon, R., 2013. Rate based modeling for CO_2 absorption using monoethanolamine solution in a hollow fiber membrane contactor. J. Membrane Sci. 429, 396–408.
Rongwong, W., Fan, C., Liang, Z., Rui, Z., Idem, R.O., Tontiwachwuthikul, P., 2015. Investigation of the effects of operating parameters on the local mass transfer coefficient and membrane wetting in a membrane gas absorption process. J. Membrane Sci. 490, 236–246.
SageMath mathematics software system, v9.4 (2021-08-22), https://www.sagemath.org/
Salazar, A., Campo, A., Schuler, C., 1988. On a solution of the Graetz-Nusselt problem and its extension with uniform wall heating. Wärme Stoffübertrag 22, 141–146.
Schöner, P., Plucinski, P., Nitsch, W., Daiminger, U., 1998. Mass transfer in the shell side of cross flow hollow fiber modules. Chem. Eng. Sci. 53, 2319–2326.
Scholes, C.A., Simioni, M., Qader, A., Stevens, G.W., Kentish, S.E., 2012. Membrane gas–solvent contactor trials of CO_2 absorption from syngas. Chem. Eng. J. 195-196, 188–197.
Shah, R.K., London, A.L., 1978. Laminar flow forced convection in ducts. Academic Press.
Shah, R., 1975. Thermal entry length solutions for the circular tube and parallel plates. Paper No. HMT-11-75. In: Proc. National Heat Mass Transfer Conf., Bombay, India.
Shih, Y.-P., Tsou, J.-D., 1978. Extended Leveque solutions for heat transfer to power law fluids in laminar flow in a pipe. Chem. Eng. J. 15, 55–62.
Skelland, A.H.P., 1974. Diffusional mass transfer. Wiley, New York.
Sohaib, Q., Muhammad, A., Younas, M., Rezakazemi, M., Druon-Bocquet, S., Sanchez–Marcano, J., 2021. Rigorous non-isothermal modeling approach for mass and energy transport during CO_2 absorption into aqueous solution of amino acid ionic liquids in hollow fiber membrane contactors. Sep. Purif. Technol. 254, 117644.
Subramanian, V.R., White, R.E., 2004. Semianalytical method of lines for solving elliptic partial differential equations. Chem. Eng. Sci. 59, 781–788.
Vallero, D., 2014. Fundamentals of air pollution, 5th Edition Academic Press.
Wang, Z., Fang, M., Yan, S., Yu, H., Wei, C.-C., Luo, Z., 2013. Optimization of blended amines for CO_2 absorption in a hollow-fiber membrane contactor. Ind. Eng. Chem. Res. 52, 12170–12182.
Wang, C.Y., Mercer, E., Kamranvand, F., Williams, L., Kolios, A., Parker, A., Tyrrel, S., Cartmell, E., McAdam, E.J., 2017. Tube-side mass transfer for hollow fibre membrane contactors operated in the low Graetz range. J. Membrane Sci. 523, 235–256.
Wickramasinghe, S.R., Semmens, M.J., Cussler, E.L., 1992. Mass transfer in various hollow fiber geometries. J. Membrane Sci. 69, 235–250.
Worsøe-Schmidt, P.M., 1967. Heat transfer in the thermal entrance region of circular tubes and annular passages with fully developed laminar flow. Int. J. Heat Mass Transfer 10, 541–551.
Xu, Y., Goh, K., Wang, R., Bae, T.-H., 2019. A review on polymer-based membranes for gas-liquid membrane contacting processes: Current challenges and future direction. Sep. Purif. Technol. 229, 115791.
Yang, M.-C., Cussler, E.L., 1986. Designing hollow-fiber contactors. AIChE J 32, 1910–1916.
Yoon, S.K., Fichtl, G.W., Kenis, P.J.A., 2006. Active control of the depletion boundary layers in microfluidic electrochemical reactors. Lab Chip 6, 1516–1524.
Zheng, J.-M., Xu, Y.-Y., Xu, Z.-K., 2003. Shell side mass transfer characteristics in a parallel flow hollow fiber membrane module. Sep. Sci. Tech. 38, 1247–1267.